THE TEMPERATURE DEPENDENT ELECTRICAL CHARACTERISTICS OF Au/(n)PbS SCHOTTKY BARRIER JUNCTION FABRICATED BY CHEMICAL BATH DEPOSITION METHOD

L. RAJEN SINGH*
D. M. College of Science, Imphal-795001, Manipur, India

Nanocrystalline Manganese(Mn) doped lead sulphide (PbS) thin films are prepared by chemical bath deposition (CBD) method at bath temperature 313K using Manganese Acetate, Lead Acetate and Thiourea. The films deposited onto bare glass substrates are characterized by X-ray diffraction (XRD), Energy Dispersive X-ray analysis (EDX), scanning electron microscopy (SEM) and transmission electron microscopy (TEM) analysis. Au/(n)PbS Schottky barrier junctions are fabricated onto indium tin oxide (ITO) substrates to study the junction parameters. The Current-Voltage (*I-V*) characteristics of the junctions are measured in the temperature range 303-333 K and junction parameters are calculated. The ideality factor (n) and Schottky barrier height (ϕ_b) at different temperatures are found to vary from 6.29 to 4.88 and 0.806 eV to 0.820 eV respectively. It is observed that the ideality factor decreases while the barrier height increases with increase of temperature. Further, it is found that the series resistance R_s of the junctions are strongly temperature dependent. The carrier concentration determined from the capacitance-voltage (*C-V*) plot is found to be of the order $10^{16}cm^{-3}$.

(Received October 18, 2018; Accepted January 8, 2019)

Keywords: Nanocrystalline Mn doped PbS, CBD,XRD, EDX, SEM, TEM, Au/(n)PbS Schottky barrier junctions, Ideality factor, Schottky barrier height

1. Introduction

Different semiconducting materials are used in different solid state devices depending on their band gaps and properties. Today, the metal-semiconductor junctions are much used as rectifiers, microwave diodes, UV detectors, switching diodes, photo sensors and solar cells [1-6]. PbS is an interesting narrow band gap semiconductor having band gap (0.41 eV in bulk form) [7]. The energy band gap (E_g) of nanocrystallinePbS can be tuned to anywhere between 0.41eV (bulk) to 4 eV [8]. For these reasons, many researchers study this material by various deposition techniques such as spray pyrolysis [9], electro deposition [10,11], microwave heating [12,13], successive ionic layer adsorption and reaction (SILAR) [14], vacuum evaporation [15], molecular beam epitaxy [16], chemical bath deposition [17-20] etc. Among these methods, chemical bath deposition method has several advantages compared to other techniques such as uniform film deposition, inexpensive, convenient for large area deposition and do not require sophisticated instruments [21,22]. The dimensions of the crystallites and quality of the films can be controlled by varying the deposition parameters such as pH value, reaction time, deposition temperature, concentration of lead, manganese and sulphur ions. The deposition conditions and techniques play a major role in the physical properties of Mn doped PbS thin films.

Metal-Semiconductor (MS) contacts are the most widely used rectifying contacts in the electronics industry [23-25]. The performance and reliability of a Schottky diode is drastically influenced by the interface quality between the deposited metal and semiconductor surface [26]. The detailed measurements of the physical parameters of the Schottky barrier formed at the interface of a semiconducting colloidal quantum dot film and a metal and the ideality factor 1.3 for the Al/PbS CQD Schottky devices were reported by *Clifford et al.* [27]. *Debnath et al.* [28] have

*Corresponding author: l_rajen03@yahoo.com

reported a ITO/PbS CQD film/LIF/Metal Schottky device with fill factor 51% and efficiency 3.6%. *Strasfeld et al.*[29] fabricated planar PbS quantum dot devices with ohmic and Schottky type electrodes and investigated the vast difference between the local photocurrents that arise due to Ohmic and Schottky contacts. However, there is a limited literature on the properties of Au/(n)PbSSchotty junctions fabricated by CBD. Therefore, our main aim in this work is to study the structural and surface morphological characteristics of Mn doped PbS films and electrical characterization of Au/(n)PbS Schottky junction prepared by CBD method.

2. Experimental details

Nanocrystalline Mn doped PbS thin films were deposited onto chemically cleaned glass and ITO glass substrates by CBD method using Manganese acetate, lead acetate and thiourea as Mn^{+2}, Pb^{+2} and S^{-2} sources respectively. For this, freshly prepared 0.05M solution of lead acetate (premixed with 2 wt. % Manganese acetate) and pH value of the solution was maintained at 11 by drop wise addition of NH_3 solution. Another equal amount of 0.05 M solution of thiourea was added and the solution mixture was stirred well. Bare glass and ITO glass substrates were immersed vertically into the solution. The solutions mixture was heated at 313 K for 1 hour and then kept overnight at room temperature for further deposition. After deposition, the substrates coated with Mn doped PbS on both sides were taken out and thoroughly washed with distilled water and dried in air. The films deposited on the glass substrates were used for XRD, EDX, SEM and TEM studies. The structure of the film was obtained using X-ray diffraction (XRD) XPERT-PRO Philips diffractometer. Surface morphology of the film was studied using JEOL-JSM 6360. Transmission electron microscopy (TEM) of the Mn doped PbS sample was carried out using JEM-2100 to estimate particle size. Semiconductor-metal contacts were made by evaporating gold electrodes of area (2mm x 2mm) on the Mn doped PbS films deposited over ITO glass substrates as shown in Fig.5 (inset). A Schottky junction device in the configuration Au/(n)PbS/ITO was thus, obtained to study junction parameters. *I-V* characteristics in the temperature range 303-333 K were measured by using Keithley Electrometer (6514) and Rishabh multimeter (14S). The temperature on the sample surface was measured by Instron (IN-303) digital temperature controller using PT- 100 sensor. *C-V* measurement was carried out using Systronics LCR-Q meter (928). The type of the Mn doped PbS semiconductor as found by hot probe method was n-type. For forward bias, the negative terminal of the voltage source was connected to the ITO glass site while the positive terminal to the gold electrodes.

3. Results and discussion

3.1. Structural properties

The XRD patterns of nanocrystalline Mn doped PbS thin films deposited on the glass substrates are shown in Fig. 1. The diffraction peaks observed at 2θ values of 25.908˚, 29.923˚, 42.948˚, 50.902˚, 53.369˚, 62.510˚, 69.190˚, 71.049˚ and 78.850˚ correspond to (111), (200), (220), (311), (222), (400), (331), (420) and (422) planes respectively which are in good agreement with the JCPDS data reference code no. 01-077-0244 [30]. Therefore, it has been concluded that the deposited PbS thin films are polycrystalline in nature with cubic structure. The orientation of the grain growth is preferably along (200) direction. The preferential orientation in the (200) direction has also been reported by Gadave et al. [31] for PbS films deposited by CBD at 80˚C and by Puiso et al. [32] of SILAR deposited PbS films on Si substrates. The average crystallite size is calculated using Scherer's equation [33]

$$D = \frac{0.94\lambda}{\beta \cos\theta} \tag{1}$$

Where *k* is a constant equal to 0.94, λ is the wavelength of the x-ray used (CuK_α radiation, λ = 1.5418Å), β is the full width at half maximum (FWHM) of the dominant x-ray diffraction peak in radian and θ is the diffraction angle of the dominant peak. The average crystallite size of the Mn doped PbS was found to be 14 nm.

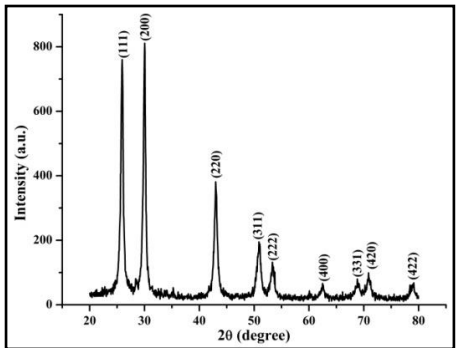

Fig.1. XRD spectra of nanocrystalline Mn doped PbS thin film.

3.2.Elemental analysis

To confirm the chemical composition of Mn doped PbS thin film, the elemental analysis of the samples were performed by Energy Dispersive X-ray Spectrometer (EDX). Fig. 2 shows a typical EDX spectrum of 2 wt.% Mn doped PbS thin film. The spectrum confirms that Pb, S and Mn atoms are present in the prepared film. The average atomic percentage of Pb, S and Mn are found to be 47.11, 50.24 and 2.65 respectively.The presence of Mn atoms in the spectra indicates that Mn atoms are incorporated with the PbS film. The extra peaks observed in the EDAX spectra correspond to some impurity elements like Mg, Si, Na, Ca which are due to glass substrate or the substrate holder used in the EDAX instrument [34-36]. These might also be due to presence of C and O due to exposure of the film to the atmosphere [37]. There is no source of these elements in the chemicals used for the Mn doped PbS film synthesis. We consider only the atomic % of Pb, S and Mn present in the spectra of doped sample neglecting the percentage of the other elements present in the spectra.

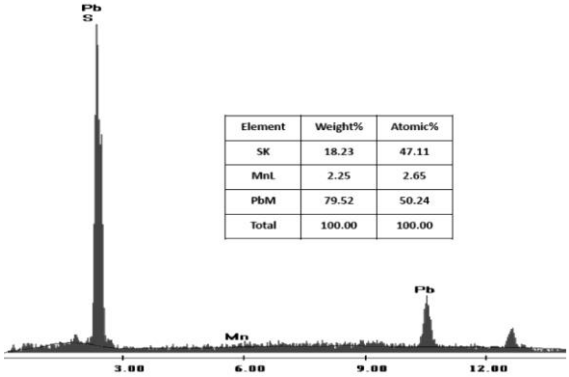

Element	Weight%	Atomic%
SK	18.23	47.11
MnL	2.25	2.65
PbM	79.52	50.24
Total	100.00	100.00

Fig.2. EDAX spectra of 2 wt.% Mn doped PbS thin prepared at concentration 0.05 M, pH value 11 and deposition temperature 313K.

3.3.SEM and TEM studies

The surface morphology of nanocrystalline Mn doped PbS thin films based on SEM image analysis is shown in Fig. 3. It is observed that the film is dense, smooth, homogeneous without any pore and consisting of grains of unequal shapes and sizes.

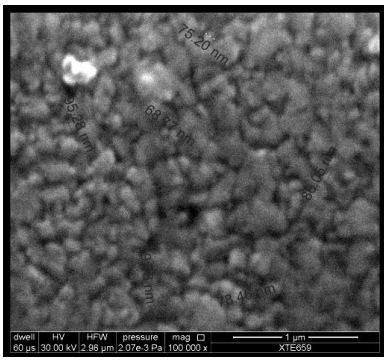

Fig.3. SEM Photographs of nanocrystalline Mn doped PbS thin film.

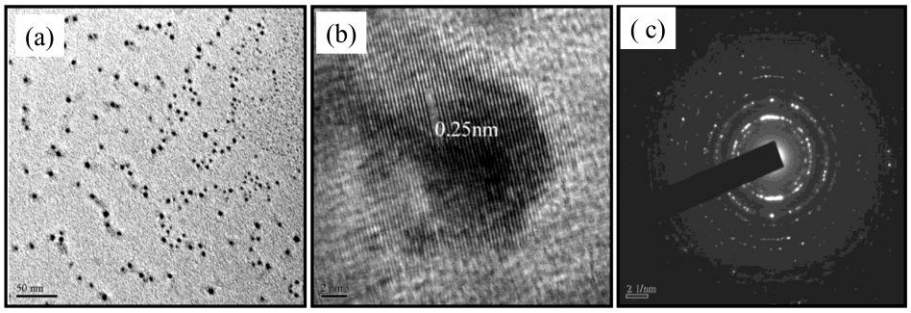

Fig.4. (a) TEM image (b) High-resolution transmission electron microscopy and (c) selected area electron diffraction images of nanocrystalline Mn doped PbS film.

Transmission electron microscopy (TEM) image of nanocrystalline Mn doped PbS thin films is shown in Fig.4. It reveals small particles attach together as well as large particles having spherical shapes. The particles in dark colour shown in Fig.4(a) are the nanocrystalline Mn doped PbS and the calculated particles size is found to be in the range of 3-13 nm which is in good agreement with the X-ray diffraction results. HRTEM is used to study the structure as well as to observe lattice images showing different orientations of the nanocrystals of Mn doped PbS. The HRTEM image shown in Fig. 4(b) exhibits lattice fringes with d-spacing of 0.25 nm corresponding to the (200) reflection of the PbS cubic phase. Selected area electron diffraction (SAED) image shown in Fig.4(c) exhibits multiple diffractions rings with missing periodicity which is due to the random orientation of the particles.

3.4. I-V characteristics of the Schottky barrier junction

The prepared Mn doped PbS thin films is a n-type semiconductor as determined by the hot probe method. Gold electrode with a work function 5.1 eV is deposited above the PbS films to form Schottky Barrier Junction between Au and PbS film. The reverse bias condition refers for Au/(n) Mn doped PbS/ITO structure to a bias voltage across the junction with positive polarity connected to the n- type PbS film through ITO electrode making Ohmic contact at the back and negative polarity to counter electrode of barrier metal Au. Fig.5 shows the energy band diagram of a typical Au/(n) Mn doped PbS Schottky barrier junction before and after formation of the contact.

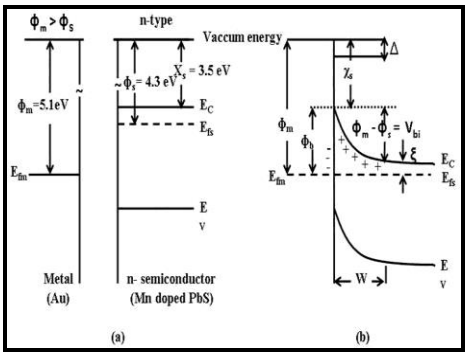

Fig. 5. Energy band diagram of Au/(n)Mn doped PbS Schottky Barrier Junction (a) before contact and (b) after contact.

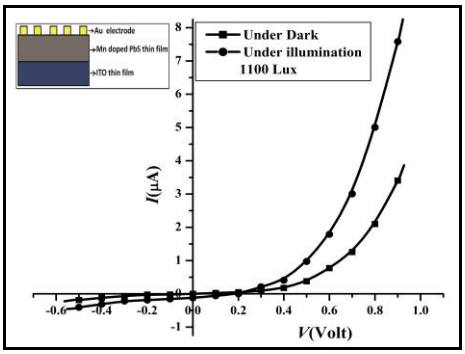

Fig. 6. I-V characteristics of a typical Au/(n)Mn doped PbS Schottky Barrier junction in dark and under illumination at room temperature (303K) and (inset) Schematic diagram of Au/(n)PbS Schottky barrier junction.

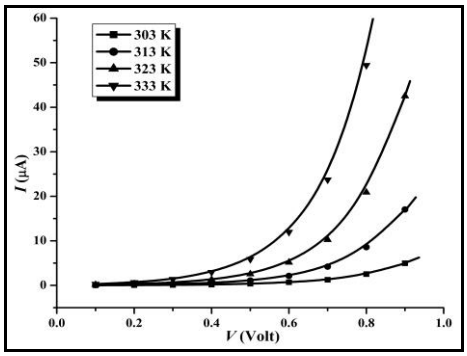

Fig.7. I-V characteristics of Au/(n)PbS Schottky Barrier Junction in dark at various temperatures.

Fig. 6 shows the *I-V* characteristics of the typical Au/(n)Mn doped PbS Schottky Barrier Junction in dark and under illumination at room temperature (303K). The junction is formed to exhibit rectifying characteristics both in dark and under illumination (1100 lux). However, the characteristics under illumination shows photovoltaic effect and are more rectifying in nature.

Fig. 7 shows the *I-V* characteristics of the typical Au/(n)PbS Schottky Barrier Junction under dark at various temperatures. It has been observed that beyond room temperature (303K), the current increases abruptly with voltage.

The non-linear forward bias current through a Schottky contact could be well described by the thermionic emission theory. According to thermionic emission theory, the current density in Schottky barrier diodes is given as

$$J = J_o \exp\left(\frac{qV}{nkT}\right)\left[1-\exp\left(\frac{-qV}{kT}\right)\right] \tag{2}$$

where J_o is the saturation current density, k is the Boltzman constant, n is the ideality factor, T is the absolute temperature, q is the electron charge and V is the applied voltage. The saturation current density J_o can be written as

$$J_o = A^* T^2 \exp\left(\frac{-q\phi_b}{kT}\right) \tag{3}$$

where A^* is the effective Richardson constant and ϕ_b is the barrier height. The ideality factor (n) and the saturation current density (J_o) of a Schottky diode is calculated from the slope of the linear region of the forward bias and the straight line intercept of Fig.8 at V=0. The equation for n can be expressed as

$$n = \frac{q}{kT}\left[\frac{dV}{d\left(\ln\left(\frac{J}{1-e^{-qV/kT}}\right)\right)}\right] \tag{4}$$

Fig. 8 shows the linear portions of the $\ln\{J/(1-e^{-qV/kT})\}$ vs V plots of the typical Au/(n)PbS Schotky Barrier Junction at different temperatures ranging from 303K to 333K. The values of the saturation current density and ideality factor of the junctions at different temperatures are calculated from these plots and are given in Table 1.

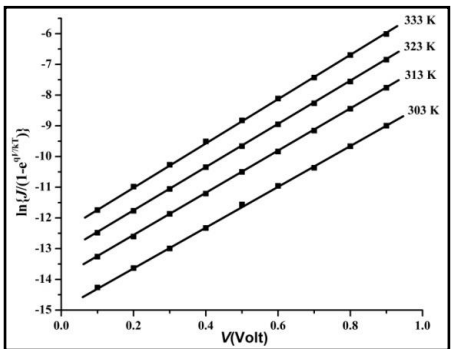

Fig.8. $\ln\{J/(1-e^{-qV/kT})\}$ *versus V plots of the typical Au/(n)PbS Schottky Barrier Junction at different temperatures in dark.*

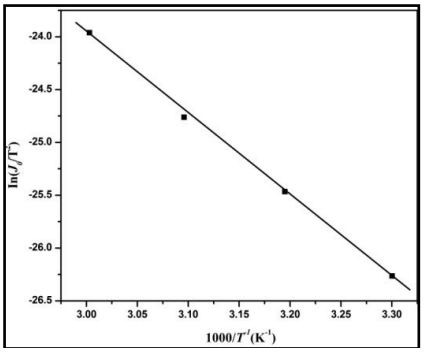

Fig. 9. In (J_o/T^2) versus T^{-1}plots at different temperatures in dark of the typical Au/(n)PbS Schottky Barrier Junction.

The ideality factor (n) is observed to decrease while the saturation current density J_o is found to increase with increase of temperature for the typical junction. The increase in saturation current with temperature is due to the fact the the current transport mechanism is dominated by thermionic emission process (38). The calculated values of J_o at different temperatures are used to draw $\ln(J_o/T^2)$ vs T^{-1}(Richardson plot).

Fig. 9 shows such Richardson plot for the typical junction. Table 1 shows the calculated values of Richardson constant (A^*) and barrier heights of the typical junction. The barrier heights measured from these Richardson plots are found to increase 0.808 eV to 0.832 eV for the typical Au/(n)PbS Schottky Barrier Junction. The increase in barrier heights with temperature is due to the inhomogeneous distribution of barrier heights at the metal semiconductor interface (39).

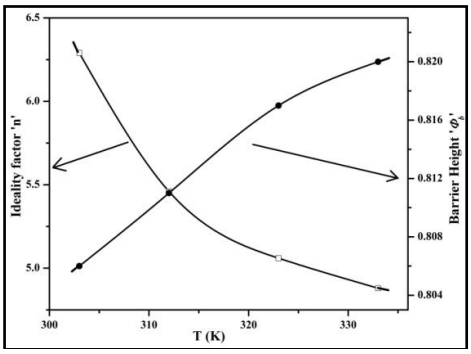

Fig. 10. Plots of Ideality factor (n), Schottky Barrier Height (ϕ_b) with temperature (T) for the typical Au/(n)PbS Schottky Barrier Junction (a) as-prepared and (b) after heat treatment.

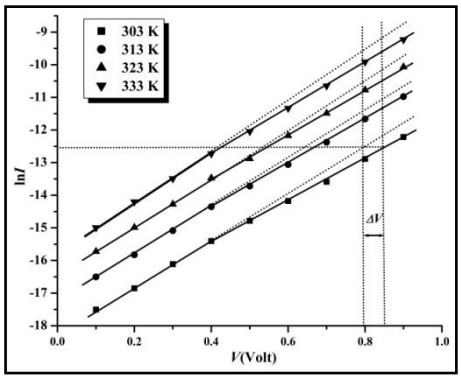

Fig.11. Plot of lnI versus V of Au/(n)PbS Schottky barrier junction at different temperature.

Fig. 10 shows temperature variation of the ideality factors (n), Schottky Barrier height (ϕ_b) for the typical junction as-prepared and after heat treatment. It is observed that the Barrier height (ϕ_b) increases with the increase of temperature while the diode ideality factor (n) decreases with the increase of temperature.

From the study, it is observed that both the Saturation current density (J_o) and the Barrier height (ϕ_b) increases with the increase of temperature while the diode ideality factor (n) decreases with the increase of temperature.

3.5. Series resistance

The Plot of *lnI* versus *V* of Au/(n)PbS Schottky barrier junction at different temperatures deviate from the straight line as shown in Fig.11 and this is due to the presence of series resistance (R_s) associated with the region between the depletion region and Ohmic contact. Here the voltage drop across R_s causes the actual voltage developed across the barrier region to be less than the

applied voltage to the junction. The values of R_s obtained by plotting ΔV vs I (as shown in Fig. 12) are given in Table 1. The series resistances so obtained are found to be in the order of KΩ. The decrease in value of R_s with increasing temperature is due to an increase in the number of free charge carriers by bond breaking [40].

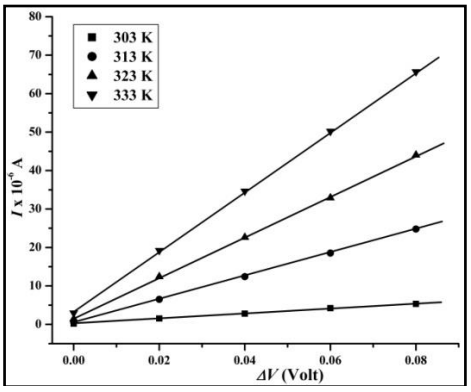

Fig. 12. Plot of I vs ΔV plots) of the typical Au/(n)PbS Schottky barrier junction at different temperatures.

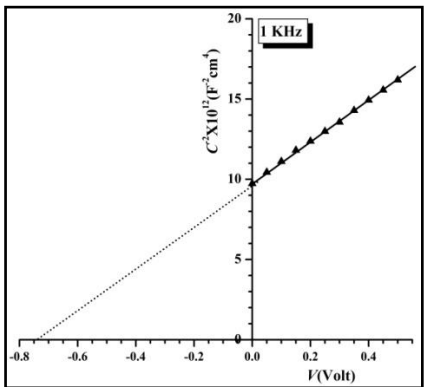

Fig.13. Plot of C^{-2} versus V for Au/(n)PbS Schottky Schottky barrier junction at room temperature 303K.

Table 1. Junction parameters of Au/(n)PbS junction at different temperatures.

Temperature (K)	Saturation current density J_o (Acm^{-2})	Ideality factor (n)	Potential barrier height (ϕ_b) eV	Series resistance R_s(KΩ)	Carrier concentration (N_a) cm^{-3}	Richardson Constant A^* ($Acm^{-2}K^{-2}$)
303	0.361 x 10^{-6}	6.29	0.808	14	6.79 x 10^{16}	98
313	0.854 x 10^{-6}	5.46	0.813	3		
323	1.840 x 10^{-6}	5.06	0.820	2		
333	4.351 x10^{-6}	4.88	0.832	1		

3.6. C-V characteristics of the Schottky barrier junction

The reverse bias C^{-2} versus V plot of the Au/(n)PbS junction measured in the room temperature (303K) at a frequency of 1 KHz is shown in Fig.13.

The depletion layer capacitance in Schottky barrier diode is expressed as [41]

$$C = \left(\frac{q\varepsilon_s N_a}{2}\right)^{\frac{1}{2}} \left(V_d - \frac{kT}{q}\right)^{\frac{-1}{2}} \tag{6}$$

where $\varepsilon_s = 160\varepsilon_o$ is the permittivity of the PbS [37], $\varepsilon_o = 8.854 \text{ X } 10^{-12}$ and N_a = acceptor density or the carrier concentration. Since, the diffusion potential, $V_d = V_{bi} + V_r$, where V_{bi} is the diffusion potential at zero bias, the above expression for C may be written as

$$C = \left(\frac{q\varepsilon_s N_a}{2}\right)^{\frac{1}{2}} \left(V_{bi} + V_r - \frac{kT}{q}\right)^{\frac{-1}{2}} \tag{7}$$

$$\frac{1}{C^2} = \frac{2\left(V_{bi} + V_r - \frac{kT}{q}\right)}{q\varepsilon_s N_a} \tag{8}$$

$$d\left(\frac{1}{C^2}\right) = d(C^{-2}) = \frac{2d(V_r)}{q\varepsilon_s N_a} \tag{9}$$

$$N_a = \frac{2d(V_r)}{q\varepsilon_s d\left(C^{-2}\right)} \tag{10}$$

The plot of C^{-2} versus V, according to equation (9) will give a straight line with a

$$Slope = \frac{2}{q\varepsilon_s N_a} \tag{11}$$

From eqn. (8), at $C^{-2} = 0$, the intercept is

$$V_i = -V_r = V_{bi} - \frac{kT}{q}$$

$$V_{bi} = V_i + \frac{kT}{q} \tag{12}$$

The diffusion potential, V_{bi} is determined by knowing V_i from the plot (Fig.13) and found to be 0.786eV. The carrier concentration N_a obtained by using (10) is $5.075 \text{ X } 10^{16}/\text{cm}^3$. As the barrier height ϕ_b is the sum of the diffusion potential V_{bi} and ξ, this can be calculated from the equations

$$\xi = \frac{kT}{q} \ln\left(\frac{N_c}{N_d}\right) \tag{13}$$

$$\phi_b = V_i + \xi + \frac{kT}{q} \tag{14}$$

where $N_c = 2\left(2\pi m_e^* \frac{kT}{h^2}\right)^{\frac{3}{2}}$ is the effective density of states in the conduction band for PbS at room temperature, N_d is the doping concentration calculated from the slopes of $C^{-2} - V$ plots

(Fig. 13), *h* is the Planck's constant, *k* is the Boltzmann's constant and m_e^* is the effective electron mass for PbS given by $m_e^* = 0.080 m_o$ where m_o is the rest mass of electron [42]. Thus, the barrier height ϕ_b obtained from the C-V plot is 0.81eV. The barrier height ϕ_b obtained from I-measurements at room temperature is lower than those obtained from C-V measurements. The difference may be due to the formation of an interfacial layer containing defects. Thus, interfacial capacitance and capacitance due to depletion layer are in series, thereby decreasing the total capacitance and as a result, C^{-2} increases. This increases the intercept of C^{-2} versus V plot and increases the barrier height which may be due to the transport mechanism in these diodes and it is purely thermionic emission in nature. Another reason may be the lowering of barrier height by the image force due to current flow across the barrier. In view of the fact that the I-V method involves the flow of electrons from semiconductor to the metal, the barrier height determined from the I-V method will logically yield lower barrier heights than the C-V measurements [43].

Conclusions

Nanocrystalline Mn doped PbS thin film is prepared and deposited on ITO glass substrate by CBD method and Au/(n)Mn doped PbS Schottky Barrier junction is fabricated using Au electrode deposited by vacuum evaporation over the Mn doped PbS film on ITO glass substrate. SEM results reveal that the overall surface morphology of the film is fairly smooth and uniform. The films consist of particles of different shapes and sizes. The particle size determined from XRD and TEM are closely agreed. The current-voltage characteristics of the junction at different temperatures are investigated. The ideality factor decreases and the potential barrier height increases with increase in temperature. These observations have been ascribed to barrier in homogeneities at the metal-semiconductor interface. The calculated series resistance R_s at different temperature is found to be in the range from 14 KΩ to 1 KΩ. The value of R_s decreases with increasing temperature due to increase in the number or density of free charge carriers by bond breaking. The barrier height determined from the C-V is larger than those obtained from I-V characteristics. The carrier concentration N_a obtained from the C-V is found to be in the order of $10^{16}/cm^3$.

Acknowledgments

I express my gratitude to IIT. Guwahati, India for EDX analysis, Department of Physics, Manipur University, Manipur, India, Department of instrumentation & USIC,Gauhati University, Guwahati, India for providing XRD, SEM and lastly SAIF, NEHU, Shillong, India for TEM analysis.

References

1. Yu-ZungChiou, Yan-Kuin Su, Shoou-Jinn Chang, Jone F. Chen, Chia-Sheng, ChanSen Hai Liu, Yi-Chao Lin, Chin-Hsiang Chen, Jpn. J. Appl. Phys.**41**, 3643(2002).
2. T. Tsutomu, O. Shigeki, K. Kazuo, F.Junji, Jpn. J. Appl. Phys. Pt. **24**, 593 (1985).
3. Chen, C. H. Chang, S. J. Su, Y. K. Chi, G. C. Chi, J. Y. Chang, C. A. Sheu, J. K. Chen, Photonics Technology Letters, IEEE **13**, 848 (2001).
4. F. D. Shepherd, A. C. YangJr., International Electron Devices Meeting**19**, 310 (1973).
5. Chih-TangnSah, Fundamentals of Solid State Electronics, World Scientific (Electronicbook- www.worldscincebook.com) (1991).

6. Boylestad, Nashelsky, Electronic Devices and Circuit Theory, PenticeHallofIndia, New Delhi, 2003.
7. M. Navaneethan, K. D. Nisha, S. Ponnusamy, C. Muthamizhchelvan, Rev. Adv. Mater.Sci.**21**, 217 (2009).
8. N. B. Kotadiya,A. J. Kothari, D. Tiwari, T. K. Chaudhuri,Appl. Phys A **108**,819(2012).
9. B. Thangaraju, P. Kaliannan, Semiconductor Science and Technology**15**, 849 (2000).
10. P. Raji, C. Sanjeeviraja, K. Ramchandran, Bull. Mater.Sc. **28**(3), 233 (2005).
11. R. Sahraei, R.Shahriyar, S.Majles, M. H. Ara, A. Daneshfar, N. Shokri, Prog. Colour colourants Coat.**3**,82 (2010).
12. Gary Hodes, Chemical Solution Deposition of Semiconductor Films, Marcel Dekker, Inc. 2002.
13. S. Mageswari, L. Dhivya, B. Planivel, R.Murugan, Journal of Alloys and Compounds **545**, 41 (2012).
14. R. K. Joshi, A. Kanjilal, H. K. Sehgal, Nanotechnology**14**, 809 (2004).
15. N. F. Mott, E. A. Davis, Electronics Processes in Non-CrystallineMaterials, Clarendon, Oxford, p 428, 1979.
16. V. I. Levchenko, L. I. Postnova, V. P. Bondarenko, N. N. Vorozov, V. A. Yakovtseva, L. N. Dolgyi, Thin solid films**348**, 141 (1999).
17. S. Seghaier, N. Kamoun, R. Brini, A. B. Amara, Mater. Chem. Physics. **97**,71 (2006).
18. J. J. V. Jauregu, R. R. Bon, A. M. Galvan,M. S. Lerma, Thin Solid Films**441**, 104(2003).
19. E. Pentia, L. Pintillie, C. Tivarus, I. Pintillie, T. Botila, Mater. Sci. Eng. B**80**, 23(2001).
20. R. K. Joshi, A. Kanjilal, H. K. Sehgal, Appl. Surf. Sci. **221**,43(2004).
21. K. M. Gadave, S. A. Jodgudri, C. D. Lokhande, Thin Solid Films **245**,7(1994).
22. S. Bhushan, M. Mukharjee, P. Bose, J. Mater. Sci. Mater. Electron.**13**, 581(2002).
23. E. H. Rhoderick, R. H. Williams, Metal-Semiconductor Contacts, Clarendon Press, Oxford University Press, Oxford, 1988.
24. H. Cetin, E. Ayyildiz, Semiconductor. Sci. Technology**20**,625(2005).
25. R. L. Van Meirhaeghe, W. H. Laflere, F. Cardon, J. Appl.Physics.**76**,403(1994).
26. E. Gur, S. Tuzeman, B. Kilic, C. Coskun, J. Phys. Condens. Matter.**19**,196(2007).
27. Jason P. Clifford, K. W. Johnston, L. Levina, E. H. Sargent, Appl. Phys. Lett. **91**, 253117 (2007).
28. R. Debnath, J. Tang, D. Aaron Barkhouse, Xihua Wang, A. G. Pattantyus-Abraham, L. Brzozowski, L,Levina, E. Sargent, Amer.Chem. J. **132**, 5952 (2010).
29. D. David Strasfeld, A. Dorn, D. D. Wanger, G. MoungiBawendi, Nano.Lett.**12**, 569 (2012).
30. Powder Diffract. File, JCPDS Internat. Centre Diffract. Data, PA 19073-3273, U.S.A., 2001.
31. K. M. Gadave, S. A. Jodgudri, C. D. Lokhande, Thin Solid Films **245**,7(1994).
32. J. Puiso, S. Tamulevicius, G. Laukaitis, S. Lindross, M. Leskeia, V. Snitka, Thin Solid Films **403**, 457 (2002).
33. B. D. Cullity, Elements of X-ray Difrraction, Massachusetts: Addison-Wesley, 102(1956).
34. Juan Chu, Zhengguo Jin, Shu Cai, Jingxia Yang, Zhanglian Hong, Thin Solid Films **520**,182 (2012).
35. R. Sahraei, S. Shahriyar, M. H. Majles Ara, A. Daneshfar, N. Shokri, Prog. Color Colorants Coat.**3**, 82 (2010).
36. S. Prabahar, M. Dhanam, Journal Crystal Growth**285**, 41 (2005).
37. S. Mageswari, L. Dhivya, B. Palanivel, R. Murugan, Journal of Alloys and Compounds**545**, 41 (2012).
38. S. M. Sze, Physics of Semiconductor Devices, 2nd Edn, Willey Eastern Ltd, New Delhi, 251, 1986.
39. A. Ahaitouf, H. Srour, S. OuldSaad Hamady, N. Fressengeas, A. Ougazzaden, J. A. Salvestrini, Thin Solid Films **522**, 345 (2012).

40. V. Janardham, H. K. Lee, K. H. Shim, H. B. Hong, S. H. Lee, K. H. Ahn, C. J. Choi, J. Alloys Compd.**504**, 146 (2010).
41. A. A. Qidwai, Journal of Engineering and Sciences, July-December, 8 (2010).
42. T. Torimoto, H. Uchid, T. Sakata, H.Mori, H. Yoneyama, J. American Chem. Soc. **115**, 1874 (1993).
43. V. L. Devi, I. Jyothi, V. R. Reddy, C. Choi, The Open Applied Physics Journal **5**, 1 (2012).